Proceedings of The Fifteenth (2005) International Offshore and Polar Engineering Conference
Seoul, Korea, June 19–24, 2005

ISBN 1-880653-64-8 (Set); ISSN 1098-6189 (Set)

Numerical Modeling of Nonlinear Surface Waves caused by Surface Effect Ships Dynamics and Kinematics

Hong Gun Sung[1] *and Stephan T. Grilli*[2]
[1] Korea Ocean Research and Development Institute, Daejeon, Korea
[2] Department of Ocean Engineering, University of Rhode Island, Narragansett RI, USA

ABSTRACT

We model fully nonlinear free surface waves caused by a translating disturbance made of a pressure patch and/or a surface-piercing body (ship), within the framework of potential flow theory. The three-dimensional higher-order Boundary Element Model by Grilli et al. (2001) and Fochesato et al. (2004) is utilized with some recent extensions. In addition to the regular Eulerian-Lagrangian updating of the free surface geometry and potential, based on higher-order explicit Taylor series expansions, a pseudo-Lagrangian updating algorithm is developed to express and solve the problem in a coordinate system traveling at the instantaneous speed of the moving disturbance. This paper presents theoretical developments and applications illustrating both the accuracy and efficiency of the present method for a traveling pressure patch and an advancing Wigley hull. Based on numerical results, it is concluded that the present numerical approach, with a pseudo-Lagrangian updating and a higher-order BEM provides accurate and efficient results.

KEY WORDS: Fully nonlinear surface waves; numerical wave tank; boundary element method; three-dimensional flows; ship waves.

INTRODUCTION

Despite some recent progress, the numerical modeling of wave generation and propagation around ocean going ships, and corresponding wave resistance, still poses significant technical problems, particularly for high-speed Surface Effect Ships (SES) such as the recently proposed Harley FastShip, for which nonlinearities in the generated wave field may be large.

Surface vessels generate so-called Kelvin wave patterns, that can radiate far downstream of the vessel. The history of wave analysis around moving ships can be traced back to Michell, Havelock, Wehausen, and other precursors of naval hydrodynamics. Most of these classical works deal with some aspects of and definition of "wave resistance", or the theoretical prediction of wave resistance of simple bodies, or ship hulls having simplified analytic lines (Wehausen, 1973). A review of analytical representations of ship waves can be found in Noblesse (2000).

When it comes to numerical computations for wave resistance, the Boundary Element Method (BEM), also originally referred to as "panel method", has been widely used since the pioneering works of Hess and Smith (1964) and Dawson (1977). In the present work, we briefly review the state-of-the-art in computational methods for the ship wave resistance problem and make some recommendations for new developments, in light of our past experience with three-dimensional (3D) BEM computations of nonlinear free surface flows (e.g., Grilli et al., 2000, 2001). Specifically, we show how our existing 3D-BEM model can be modified to simulate ship wave resistance, and how successive stages in the implementation of this modified model will be validated through comparing results to those of some benchmark cases (e.g., wave resistance due to a moving pressure patch and that of a Wigley ship hull). Our ultimate goal is to simulate wave resistance for more complex cases such as the Harley SES.

Although some methods based on a direct solution of Navier-Stokes equations have been recently proposed, mostly to address the problem of friction resistance of a ship hull, potential flow theory is still the most widely used and accurate formalism for ship wave resistance problems. Moreover, the wave resistance has usually been formulated as a steady wave flow problem. As pointed out in Sclavounos et al. (1997), the steady flow not only yields wave resistance, but also ship sinkage and trim, which are significant factors in determining power requirements and operating condition of a ship hull. Following initially mostly analytical methods, more practical and quantitative results were recently obtained due to the advent of modern computers. By the late 1970's, the so-called Neumann-Kelvin approach was beginning to be used for predicting zero or non-zero forward speed problems. In the Neumann-Kelvin (NK) approach, the body boundary condition is applied on the mean position of the exact body surface with the linearized free surface boundary conditions. As indicated in Beck and Reed (2001), the first practical application of NK to utilize the BEM can be traced to Hess and Smith (1964). It is noted that many research papers refer to the BEM as "panel method" because piecewise constant or linear quadrilateral geometry and field representations have been more widely used in numerical computations of the wave resistance of conventional ships. A further refinement has been to use the exact hull boundary condition but still with linearized free surface boundary conditions. This approach did not gain popularity, and Dawson (1977) devised the "double-body" or "Dawson's approach", where linearization is done about the double-body flow. Thus, free surface boundary conditions are dependent upon the double-

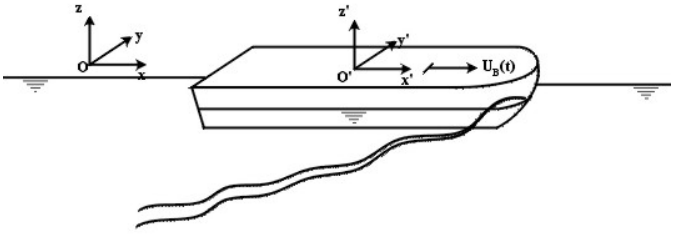

Figure 1: Sketch of problem definition

body flow. An improvement of Dawson's approach is the weak-scatter hypothesis of Pawloski (1991). The wave disturbance by the ship motion is linearized around the ambient waves with the exact ship hull boundary condition. Huang and Sclavounos (1998) utilized this approximation in developing their model SWAN4.

The Fully Nonlinear Potential Flow (FNPF) approach does not require any kind of approximation of the body nor of the free-surface boundary conditions. For the steady forward motion, initial results of using this approach can be found in Jensen et al. (1989) and Raven (1998). For unsteady ship wave problems, a time marching scheme must be used which, as indicated by Beck and Reed (2001), gives rise to many difficult problems, particularly in the mixed Lagrangian-Eulerian representation that was made popular for the study of overturning waves (Longuet-Higgins and Cokelet, 1976; Grilli and Subramanya, 1996; Grilli et al., 2001). Among these difficulties, the local treatment of breaking waves generated around the ship bow and stern particularly for high-speed ships is a very important one. To be able to pursue numerical simulations using a FPNF-BEM, beyond wave breaking, local absorption of wave energy in regions of the free surface having nearly breaking waves must be implemented. In this respect, some success was reported by Beck (1999) and, more recently, using a spilling breaker model, by Muscari and Di Mascio (2004).

Even though the use of BEM is prominent, one finds attempts to use other methodologies, such as the finite difference method (Wyatt, 2000; Park et al., 2001; Hinatsu and Hino, 2002). To our knowledge, however, field discretization methods are advantageously applied to ship hydrodynamics only when predicting viscous resistance, but are not as accurate and efficient as FNPF-BEM based methods to predict wave resistance. The present work deals with the application of an existing 3D-FNPF-BEM model (Grilli and Horrillo, 1997; Grilli et al., 2000, 2001), to the computations of the wave resistance of a high speed SES vessel such as the Harley FastShip. Some extensions of the model current capabilities are proposed as well as some new developments.

In the following sections, the mathematical and numerical formulations of the model are presented. The case of a traveling pressure patch is presented, followed by that of a Wigley-type hull, in the last section.

MATHEMATICAL FORMULATION

Governing Equations

Fig. 1 shows a sketch of the problem definition. A surface vessel on the free surface is moving/translating at a high speed in still water. Here, the shape of the body we are eventually interested in is that of a Harley SES FastShip, which is a new type of SES with catamaran hulls. The present study's long term goal is to accurately and efficiently predicting wave resistance for this type of ship.

Equations for a fully nonlinear potential flow with a free surface are listed below. The velocity potential $\phi(\boldsymbol{x},t)$ is introduced to describe the irrotational flow of an inviscid incompressible fluid, in Cartesian coordinates $\boldsymbol{x} = (x,y,z)$ with z the vertical upward direction ($z = 0$ at the undisturbed free surface), and the fluid velocity is expressed as $\boldsymbol{u} = \nabla\phi$. Continuity equation in the fluid domain $\Omega(t)$ with boundary $\Gamma(t)$ is Laplace's equation

$$\nabla^2\phi(\boldsymbol{x},t) = 0\,. \tag{1}$$

The domain boundary is composed of the free surface Γ_f, body (ship hull) boundary Γ_b, bottom boundary Γ_h, far field (downstream Γ_d or upstream Γ_u) boundaries, and vertical side boundaries Γ_s (Fig. 1). Appropriate boundary conditions must be specified on these boundaries in order to solve Eq. (1). On the free surface, ϕ satisfies the nonlinear kinematic and dynamic boundary conditions in the mixed Eulerian-Lagrangian formulation, respectively ,

$$\frac{D\,\boldsymbol{R}}{D\,t} = \boldsymbol{u} = \nabla\phi\,, \tag{2}$$

$$\frac{D\,\phi}{D\,t} = -gz + \frac{1}{2}\nabla\phi\cdot\nabla\phi - \frac{p_a}{\rho}\,, \tag{3}$$

with $\boldsymbol{R}$ being the position vector of a fluid particle on the free surface, g the acceleration due to gravity, p_a the atmospheric or applied pressure on the free surface (e.g., SES cushions), ρ the fluid density and $D/Dt = \partial/\partial t + \nabla\phi\cdot\nabla$ the Lagrangian time derivative. The effects of surface tension are neglected.

In a following section, we detail boundary conditions used for absorbing waves at truncated boundaries (Fig. 1) or for extracting wave energy on the free surface for near breaking waves, to pursue numerical simulation.

Eq. (2) is based on the Lagrangian formulation, e.g., used by Grilli et al. (2000, 2001). If one assumes a purely Eulerian representation, the equation is expressed as a function of the free surface elevation $z = \zeta(x,y,t)$ as,

$$\frac{\partial\zeta}{\partial t} + \nabla_H\phi\cdot\nabla_H\zeta = \frac{\partial\phi}{\partial z}\,, \tag{4}$$

where ∇_H denotes the horizontal component of the gradient operator.

The body boundary condition on Γ_b states that the normal velocity should be continuous from the fluid to the body,

$$\frac{\partial\phi}{\partial n} = \boldsymbol{V}\cdot\boldsymbol{n}\,. \tag{5}$$

Here, $\boldsymbol{n} = (n_x, n_y, n_z)$ is the unit normal vector pointing outward from the fluid domain, and $\boldsymbol{V}$ is the body velocity vector, which can be expressed by considering the equations of body motion, hence, as a function of the vessel horizontal speed U_B.

On the bottom Γ_h and other fixed parts of the boundary Γ_s, a no-flow condition is prescribed as

$$\frac{\partial\phi}{\partial n} = 0\,. \tag{6}$$

The boundary conditions specified on the vertical upstream and downstream boundaries is very important for obtaining accurate and reliable numerical results. For the steady translation of a surface vessel in still water, the far field condition is of the form,

$$\lim_{r^2\to\infty}\nabla\phi = 0\,. \tag{7}$$

where r denotes radial distance. Due to the truncation of the fluid domain, one modifies the exact far field condition (7) into Eq. (6), i.e., a no wave condition expressing that waves will be essentially traveling downstream. This also implies that $\phi = 0$ on Γ_u. It is worth mentioning

that Hino (1989) used the zero gradient condition (7) from the inside on the outflow and side boundaries in his finite difference solution of Navier-Stokes equations. It is noted that all the above equations are stated in earth-fixed coordinates. In order to improve numerical efficiency, however, a reference frame moving with the vessel is introduced, as explained in a following section.

Moving Computational Domain Approach

To obtain a long time history or a steady-state solution for the ship wave generation and propagation problem, when using a time domain simulation approach, one needs a very long computational domain when using an earth-fixed coordinate system. Furthermore, grid resolution should be very dense around the ship, to capture the higher waves generated around the bow and stern. Such calculations may be very time-consuming and inefficient for very large finely discretized computational domains. A practical solution to this problem is to use a coordinate system following the ship motion.

In considering the motion of the ship hull, the velocity of the moving frame corresponds to the mean speed of translation of the ship. Let the earth-fixed coordinates be $Oxyz$, and corresponding time coordinate t, and the moving reference frame $O'x'y'z'$ and the associated time t' (Fig. 1). If the speed of translation in the axis of heading is $U_B(t)$, the relation between the coordinates systems is,

$$x' = x - \int_0^t U_B(\tau)\,\mathrm{d}\tau \quad , \quad y' = y \ , \ z = z' \ , \ t' = t \tag{8}$$

Using this relation, the following equations can be used to transform the governing equations and boundary conditions to the moving system,

$$\frac{\partial}{\partial t} = \frac{\partial}{\partial t'} - U_B(t)\,\frac{\partial}{\partial x'} \ , \ \frac{\partial}{\partial x} = \frac{\partial}{\partial x'} \tag{9}$$

With these relations we find $\nabla = \nabla'$ and,

$$\frac{D}{D\,t} = \frac{D}{Dt'} - U_B(t)\,\frac{\partial}{\partial x'} = \frac{\partial}{\partial t'} + \{\nabla\phi - U_B(t)\,\boldsymbol{i}\}\,\nabla \tag{10}$$

where $(\boldsymbol{i}, \boldsymbol{j}, \boldsymbol{k})$ are the unit vector along the coordinate system axes directions.

In the moving coordinate system, the evolution of the free surface (2)-(3) is expressed with a pseudo-Lagrangian updating scheme, in which fictitious fluid particles keep a constant relative horizontal position as,

$$\begin{aligned} \frac{\tilde{D}\boldsymbol{R}}{\tilde{D}t'} &= W_y\,\boldsymbol{j} + W_z\,\boldsymbol{k} \\ \frac{\tilde{D}\phi}{\tilde{D}t'} &= \phi_t + W_y\,\frac{\partial\phi}{\partial y} + W_z\,\frac{\partial\phi}{\partial z}\,, \end{aligned} \tag{11}$$

where the pseudo-Lagrangian velocity on the free surface is $\boldsymbol{W} = (W_x, W_y, W_z)$, with,

$$W_x = U_B(t) \ , \ W_y = \frac{\partial\phi}{\partial y} \ , \ W_z = \frac{\partial\phi}{\partial z} - \frac{n_x}{n_z}\left\{U_B - \frac{\partial\phi}{\partial x}\right\} \tag{12}$$

Intersection points between the free surface and the vessel must also me updated a proper way. Various equations describing the fluid velocity at such intersection points have been proposed (Grilli and Subramanya, 1996; Shirakura et al. 2000; Liu et al. 2001). Here, we propose the following boundary conditions, for the position and velocity potential at intersection points, that also implicitly specify the body boundary condition,

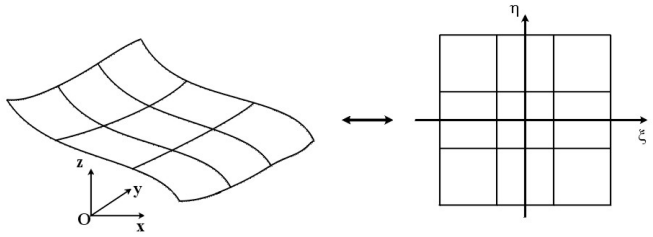

Figure 2: Sketch of 16-node cubic 3D-MII element and its corresponding reference element

$$\begin{aligned} \frac{D^*\boldsymbol{R}_I}{D^*t'} &= \left\{(\nabla\phi_I - U_B\,\boldsymbol{i})\cdot\boldsymbol{s}_B\right\}\boldsymbol{s}_B + \\ &\quad \left\{(\nabla\phi_I - U_B\,\boldsymbol{i})\cdot\boldsymbol{m}_B\right\}\boldsymbol{m}_B + \left\{\boldsymbol{V}_R\cdot\boldsymbol{n}_B\right\}\boldsymbol{n}_B \\ \frac{D^*\phi_I}{D^*t'} &= \frac{\partial\phi_I}{\partial t'} + \frac{D^*\boldsymbol{R}_I}{D^*t'}\cdot\nabla\phi_I \end{aligned} \tag{13}$$

with $\nabla\phi_I$, the fluid velocity at the intersection point $\boldsymbol{R}_I$, defined in the associated free surface element. Vectors $\boldsymbol{s}_B$, $\boldsymbol{m}_B$, and $\boldsymbol{n}_B$ are tangential and normal vectors in the body boundary element at the intersection point. Finally, $\boldsymbol{V}_R$ is the relative velocity of body motion defined as,

$$\boldsymbol{V}_R = V_z(t)\,\boldsymbol{k} + \theta_y(t)\left\{(z - z_G)\,\boldsymbol{i} - (x - x_G)\,\boldsymbol{k}\right\} \tag{14}$$

where V_z is the ship heave velocity and θ_y the ship pitch angular velocity. More detailed expressions of the updating algorithm for the intersection points are given in the Appendix.

NUMERICAL METHODS

Higher-order Boundary Element Method

The governing equation (1), with time-dependent nonlinear boundary conditions, is solved with the higher order three-dimensional (3D) FNPF-BEM model of Grilli et al. (2000,2001) extended to a moving body problem. These references should be consulted for the numerical details of the method. For a more complete understanding of the work in the context of this report, the essential aspects of the higher order BEM are given below. At the same time, model modifications and present state of development are described in detail.

Green's second identity transforms Eq. (1) into the BIE

$$\alpha(\boldsymbol{x}_l)\phi(\boldsymbol{x}_l) = \int_\Gamma \left\{\frac{\partial\phi}{\partial n}(\boldsymbol{x})G(\boldsymbol{x},\boldsymbol{x}_l) - \phi(\boldsymbol{x})\frac{\partial G}{\partial n}(\boldsymbol{x},\boldsymbol{x}_l)\right\}\mathrm{d}\Gamma\,, \tag{15}$$

where $\alpha(\boldsymbol{x}_l) = \frac{1}{4\pi}\theta_l$ and θ_l is the exterior solid angle at point $\boldsymbol{x}_l$. The 3D free-space Green's function G is given as,

$$G(\boldsymbol{x},\boldsymbol{x}_l) = \frac{1}{4\pi r} \quad \text{with} \quad \frac{\partial G}{\partial n}(\boldsymbol{x},\boldsymbol{x}_l) = -\frac{1}{4\pi}\,\frac{\boldsymbol{r}\cdot\boldsymbol{n}}{r^3}\,, \tag{16}$$

where $r = |\boldsymbol{r}| = |\boldsymbol{x} - \boldsymbol{x}_l|$ is the distance from the source point $\boldsymbol{x}$ to the field point $\boldsymbol{x}_l$ (both on boundary Γ), and $\boldsymbol{n}$ is the outward unit vector normal to the boundary at point $\boldsymbol{x}$.

The BIE (15) is solved with the 3D-MII method (Mid-Interval-Interpolation; Grilli & Subramanya, 1996; Grilli et al., 2001), in which bi-cubic approximations of the free surface geometry and unknowns are expressed, in 4x4-node sliding elements, of which only one quadrilateral

(usually the center one) is used. Curvilinear transformations are applied to express equations onto a reference element (Fig. 2). The numerical integration for source and doublet influence coefficients is carried out following the work of Grilli et al. (2001): (1) regular integrals are calculated by a bi-directional Gauss-Legendre quadrature method, (2) weakly singular integrals, where the denominator of integrands is zero at a specific node point on the corresponding element, are handled by using a polar coordinate transformation and then numerical integration, and (3) quasi-singular integrals, where the distance becomes very small but non zero, are computed by using an 'adaptive integration' scheme in which successive subdivisions of the element are made based on distance and solid angle.

As the linear algebraic system resulting from the discretization of the BIE (15) is in general dense and non-symmetric, a generalized minimal residual (GMRES) algorithm with preconditioning is used to solve it (Saad and Schultz, 1986; Grilli et al., 2001). More recently, however, a Fast Multipole Algorithm (FMA) was implemented in the BEM model (Fochesato and Dias, 2004), which, combined with GMRES for the near field, provides a computational complexity almost proportional to the number of discretization nodes N on the boundary, for large N. The last application presented in this paper uses the FMA.

Time Integration

A second-order explicit scheme based on Taylor series expansions is used to update the position $\boldsymbol{R}$ and velocity potential ϕ on the free surface (Grilli et al., 2001). Here, in moving coordinates, we find,

$$\boldsymbol{R}(t'+\Delta t') = \boldsymbol{R} + \Delta t' \frac{\tilde{D}\boldsymbol{R}}{\tilde{D}t'} + \frac{(\Delta t')^2}{2}\frac{\tilde{D}}{\tilde{D}t'}\left\{\frac{\tilde{D}\boldsymbol{R}}{\tilde{D}t'}\right\} + O\left((\Delta t')^3\right) \quad (17)$$

$$\phi(t'+\Delta t') = \phi + \Delta t' \frac{\tilde{D}\phi}{\tilde{D}t'} + \frac{(\Delta t')^2}{2}\frac{\tilde{D}}{\tilde{D}t'}\left\{\frac{\tilde{D}\phi}{\tilde{D}t'}\right\} + O\left((\Delta t')^3\right) \quad (18)$$

where $\tilde{D}/\tilde{D}t'$ is defined in Eqs. (11), (12), $\Delta t'$ is the varying time step and all terms in the right-hand sides are evaluated at time t'. Since grid points keep their horizontal location, time step $\Delta t'$ in (17) and (18) is kept constant. Global accuracy of the numerical scheme can be assessed at any time by checking the conservation of volume and total energy.

For intersection points $\boldsymbol{R}_I$, the time marching scheme takes the same form but the pseudo-Lagrangian operator $\tilde{D}/\tilde{D}t'$ is replaced by D^*/D^*t', defined in Eqs. (13),(14).

Higher Order Spatial Derivatives

One can show that the second-order pseudo-Lagrangian time derivatives in Eqs. (17) and (18) can be expressed as a function of first- and second-order spatial derivatives: $\{\phi_s, \phi_m, \phi_n, \phi_{ss}, \phi_{sm}, \phi_{mm}, \phi_{ns}, \phi_{nm}\}$, and geometric quantities, where (s, m, n) denotes an orthogonal curvilinear coordinate system on the boundary, in which n points in the outward normal direction. Expressions of the second-order derivatives for the free surface markers and intersection points are left out due to lack of space. Normal derivatives are directly obtained from the BEM solutions of Eq. (15) for ϕ, and a similar equation for ϕ_t, with relevant boundary conditions. Tangential derivatives are calculated on the boundary in a 5x5 quartic sliding element (Grilli et al., 2001). Note, Fochesato et al. (2005), recently provided more detailed and improved formulations of tangential derivatives for the model. These are used in the present applications.

Regridding

To avoid grid clustering, regridding was used at every time step throughout the simulations. After free surface updating at time t, including the position of intersection points, assuming single-valuedness of the surface elevations, the whole free surface was projected onto a fixed elliptic grid system in the horizontal plane (i.e., $x-y$ plane). Thus, the z-components of the free surface were calculated by interpolating results obtained at neighboring grid points for the corresponding time step, onto this elliptic grid. [Note, if overturning waves occurred on the free surface, yielding multiple values for a given horizontal point, one should devise a more sophisticated procedures for regridding on the parameterized surface.]

Absorption of Nearly Breaking Waves

To continue numerical simulations beyond wave overturning, steep waves that are about to break (e.g., near the ship bow and stern) must be damped, at least locally. Beck (1999) proposed a method to extract some amount of energy from waves, similar to that developed by Grilli and Horrillo (1997) for absorbing beaches. The proposed damping is based on an "absorbing free surface pressure" to be specified in the dynamic free surface boundary condition (3), in the form,

$$p_a = \gamma\, \nu(x) \mid \nabla\phi \mid^2 \mathrm{sign}\left(\frac{\partial\phi}{\partial n}\right) \quad (19)$$

for a one-dimensional example, in which γ is a constant coefficient that defines the magnitude of the damping and the sign function ensures a suitable direction for the damping pressure. The shape function $\nu(x)$, is chosen so that the damper may be a smoothly varying patch, e.g., as,

$$\nu(x) = \frac{1}{2}\left\{1 + \cos\left\{\pi\frac{(x-x_o)}{L_o}\right\}\right\} \quad (20)$$

where x_o is the abscissa where the normalized surface curvature is exceeded (i.e., breaking criterion), and L_o is the half length of the damping zone.

Damping of Upstream Oscillations

In these computations, fictitious damping was also used to remove small oscillations occurring near the far upstream boundary when using the pseudo-Lagrangian updating method (i.e., moving computational domain). This was done by modifying time updating equations as follows,

$$\begin{aligned} \frac{\tilde{D}^d(\boldsymbol{R}\cdot\boldsymbol{k})}{\tilde{D}t'} &= \frac{\tilde{D}(\boldsymbol{R}\cdot\boldsymbol{k})}{\tilde{D}t'} - \nu^d\,\boldsymbol{R} \\ \frac{\tilde{D}^d\phi}{\tilde{D}t'} &= \frac{\tilde{D}\phi}{\tilde{D}t'} - \nu^d\,\phi \end{aligned} \quad (21)$$

Here, $(\boldsymbol{R}\cdot\boldsymbol{k})$ is the z-component of the position vector $\boldsymbol{R}$ on the free surface, suffix d refers to damping, and $\nu^d(x)$ is the damping function, defined as,

$$\nu^d(x) = \nu^d_{max}\,\tanh\left\{\gamma\,\mathrm{sign}\{U_B\}\,\frac{(x-x_s)}{l_d}\right\} \quad (22)$$

where, ν^d_{max} denotes the maximum value of the damping coefficient, γ is a growth rate, x_s is the starting abscissa for damping, and l_d is the length of the damping zone. To use this damping scheme in the time stepping algorithm, in combination with second-order Taylor series expansions (17) and (18), we also derived and used second-order terms similar to both Eqs. (21) and (22).

NUMERICAL RESULTS

theoretical Gaussian shape is assumed for the pressure patch as,

$$p_a = M(t)\frac{p_o}{4}\Big\{\tanh\alpha(x'-x_0+a)-\tanh\alpha(x'-x_0-a)\Big\} \Big\{\tanh\beta(y-y_0+b)-\tanh\beta(y-y_0-b)\Big\} \quad (23)$$

where $M(t)$ is a time tapering function.

Numerical results are normalized by setting $a=1$, $g=1$, and $\rho=1$. The relationship between dimensional and dimensionless variables is,

$$\hat{x} = \frac{x}{L}\ ,\ \hat{y}=\frac{y}{L}\ ,\ \hat{z}=\frac{z}{L}\ ,\ \hat{t}=t\sqrt{\frac{g}{L}}\ ,$$
$$\hat{\phi} = \phi\frac{\phi}{L\sqrt{gL}}\ ,\ \hat{p}=\phi\frac{p}{\rho g L} \quad (24)$$

$$\hat{x'}=\hat{x}-\int_0^{\hat{t}}\frac{U_B(\tau)}{\sqrt{gL}}\,\mathrm{d}\hat{\tau} \quad (25)$$

where L is a characteristic length and $U_B(t)$ is the traveling velocity of the pressure patch.

Wave resistance to the movement of the pressure patch is obtained as,

$$R_w=-\int_{S_{AC}} p\,n_x\,\mathrm{d}S \quad (26)$$

where S_{AC} denotes the air cushion surface area (Γ_f in the present model knowing $p=0$ outside of S_{AC}).

As detailed above, a pseudo-Lagrangian time updating algorithm was implemented to solve the problem in a coordinate system traveling at the instantaneous velocity of the moving disturbance. Here, we model surface waves generated by a disturbance accelerating from a state of rest to a constant velocity. No flow boundary conditions are applied on the downstream Γ_d, upstream Γ_u, and side wall Γ_s boundaries of the domain, which move with the same speed as the pressure patch. To avoid grid clustering, regridding is used throughout the simulations at every time step. Surface pressure damping is specified to remove small sawtooth oscillations that slowly develop around the far upstream boundary. We specify the following pressure patch parameters : $L=a$, $\hat{p_o}=0.025$, $\hat{b}=2$, $\alpha a=\beta b=5$, and $\hat{U}_B=-1$. The computational domain is 18 dimensionless units long and 10 wide, with an initial grid size, 0.2 units in each direction; time step is maintained nearly constant at $\Delta\hat{t}=0.05$, throughout computations. After more than 320 time steps, the maximum change in volume of the computational domain due to numerical errors is very small, as compared to the total fluid volume (about 0.007%), confirming the accuracy of our numerical algorithms.

Fig. 3 shows the time evolution of free surface waves around the traveling pressure patch, using the new Traveling Computational Domain (TCD) approach. Fig. 4 shows the steady state wave patterns obtained for large time, both using the original full Lagrangian updating method (fixed domain) and the new pseudo-Lagrangian one (TCD). The former method uses a fixed domain and hence the pressure patch eventually approaches the extremity Γ_u, where the upstream boundary causes fluctuations in the computed R_w value. Some fluctuations can also be seen at the downstream boundary Γ_d. These fluctuations do not occur in the TCD computations.

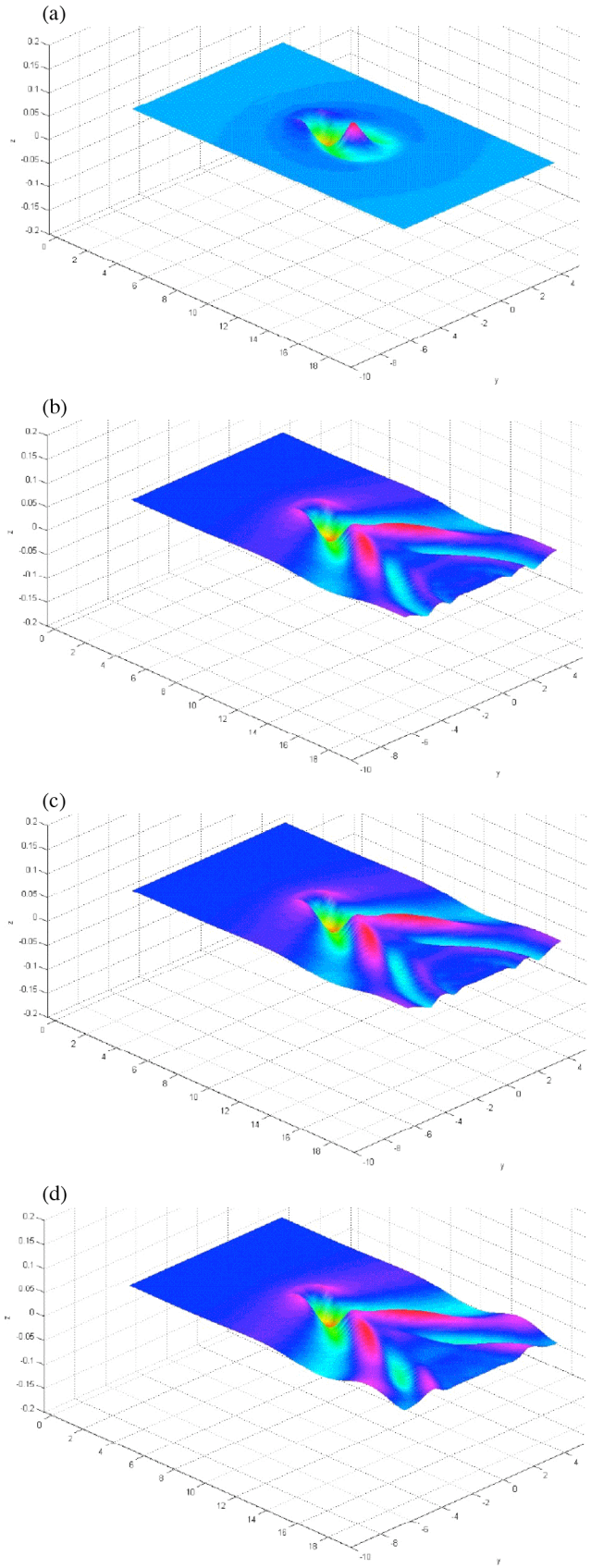

Figure 3 : Free surface evolution for the advancing pressure patch problem ($\alpha a=\beta b=5$, $\hat{U}_B=-1$), at $\hat{t}=$ (a) 4; (b) 8; (c) 12; (d) 16.

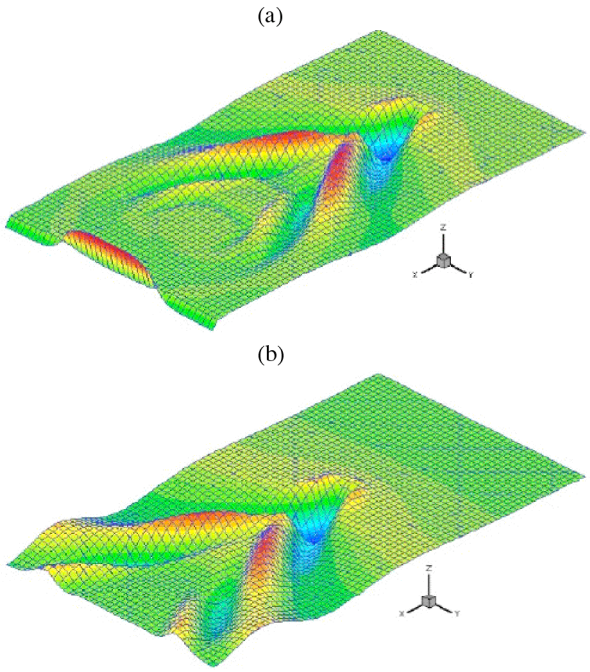

Figure 4 : Steady state free surface profiles generated by a traveling pressure patch (same case as in Fig. 3): (a) full Lagrangian updating; (b) pseudo-Lagrangian updating.

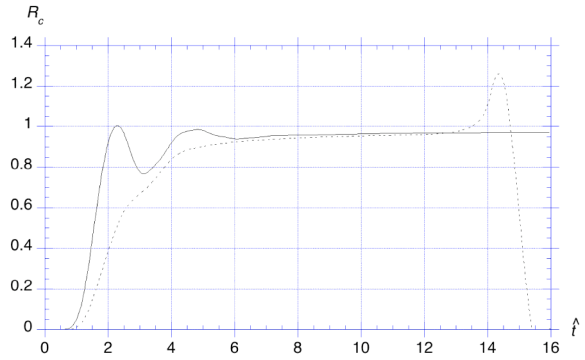

Figure 5 : Time history of wave due to the traveling pressure patch (same case as in Figure 3): pseudo-Lagrangian (——); Lagrangian (- - - - -).

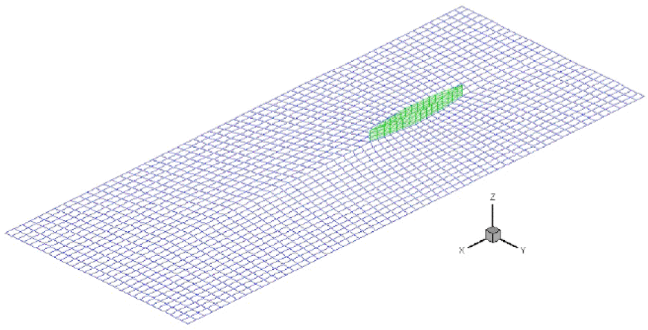

Figure 6 : Free and body surface grids for a Wigley hull.

Note, in the computations in Fig. 4a with full Lagrangian updating, an open boundary condition was specified, as a pressure sensitive "snake absorbing piston wavemaker" (Brandini and Grilli, 2001) on the downstream vertical boundary Γ_d of the computational domain. No-flow conditions were specified on other vertical boundaries. An image method was used in both cases to eliminate both the discretization on the bottom and limit computations to half the domain for symmetric cases around (Brandini and Grilli, 2001).

Fig. 5 shows a comparison of wave resistance coefficients $R_C = (R_w/W)(\rho g a/p_o)$ (with W the weight supported by the pressure patch), computed with both methods for a finite depth case : $\hat{d} = 1$. The agreement is quite good after quasi-steady state is reached $\hat{t} =$ 12-13). The predicted values of the steady state wave resistance , are : (i) 0.96 (Lagrangian updating); (ii) 0.97 (pseudo-Lagrangian updating; TCD); and (iii) 1.04 (Linear Wave Theory; Doctors and Sharma; 1972). Thus it can be concluded that the present numerical approach, with a pseudo-Lagrangian updating algorithm and a higher-order BEM provides accurate and efficient results. The advantage of the TCD approach is that one can get a steady state solution for a traveling disturbance on or beneath the free surface, with a much smaller domain. Hence, computational times are also greatly reduced.

Advancing Wigley Hull

The second application presented here is the problem of an advancing Wigley hull in calm water. The aim of this application is to check the present methodology for the case of a surface piercing body. A Wigley hull is geometrically defined as,

$$y = \pm\frac{B}{2}\left\{1-\left(\frac{2x}{L}\right)^2\right\}\left\{1-\left(\frac{z}{H}\right)^2\right\} \tag{27}$$

where L is length, B is beam, and H is draft. Since our method is fully nonlinear, we need to also define the shape of the body above the Mean Water Level $z = 0$ (MWL). The Wigley body velocity is specified as,

$$\hat{U}_B(t) = \frac{\hat{U}_B^{max}}{2}\left\{1-\cos\frac{\pi t}{T_m}\right\} \tag{28}$$

during a ramp-up time T_m, and as $\hat{U}_B = \hat{U}_B^{max}$ for later times $t > T_m$.

Fig. 6 shows the grid system used on the free surface and around the Wigley hull. Here, an elliptic grid generator is used to generate the free surface grid, and a simple algebraic gridding is applied to the body boundary.

In this application, the FMA method is used to improve computational efficiency for the solution of BEM equations with a very large number of unknowns. As before, small oscillations generated on the free surface near the upstream boundary are removed by using a simple damping technique for the free surface boundary conditions (both velocity potential and position of the free surface markers).

Intersection points between the hull and the free surface are updated with respect to the time using Eqs. (13). As we are using an explicit time stepping scheme, the updated intersection points may not always lie on the body surface. Hence, we project these points onto the body surface.

As time increases, free surface discretization nodes migrate and may accumulate around stagnation points or fast moving fluid regions having a high grid curvature. When this happens, time steps tend to decrease dramatically, due to the adaptive time step condition based on the grid Courant number, and computational time is increased. A practical and efficient treatment of this is to regrid the free surface.

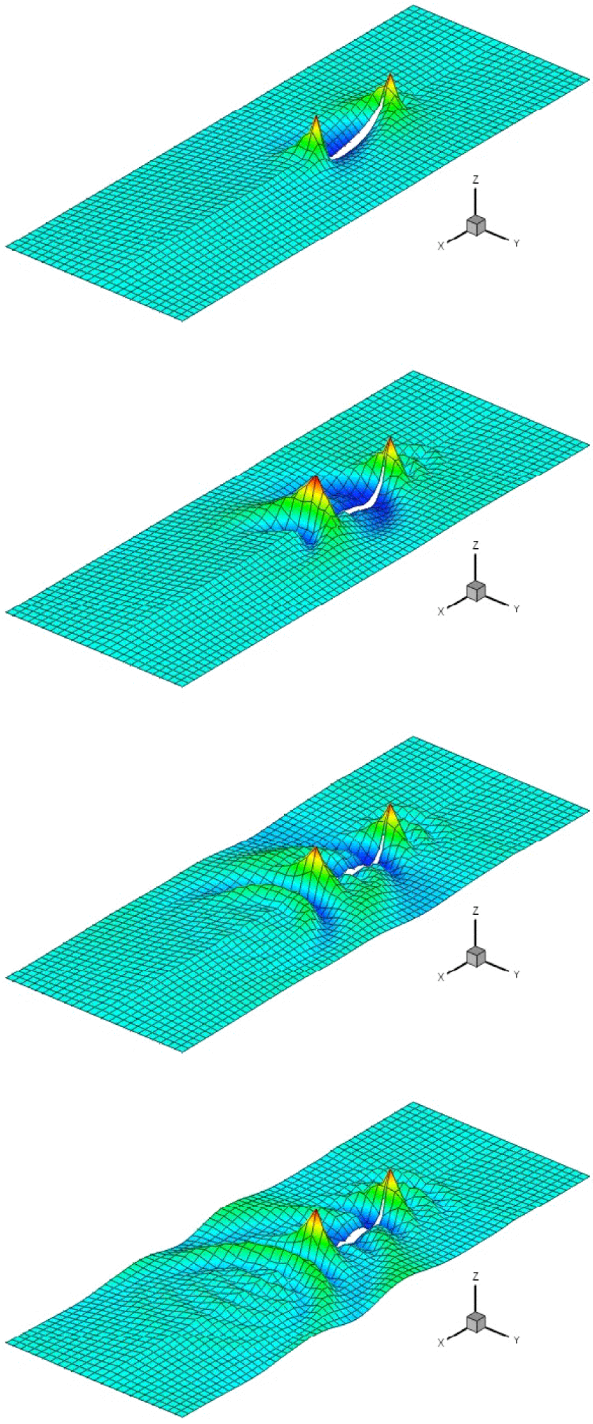

Figure 7 : Time sequence of free surface waves generated by the advancing Wigley hull for $\hat{t} = 2$, 3.5, 5, and 6.5 (last figure is for 131st time step); $Fn = 0.25$.

Fig. 7 shows preliminary results obtained for an advancing Wigley hull with $L/B = 10$ and $H/B = 6$. The Froude number is $Fn = U_B/\sqrt{gL} = 0.25$, which generates non-breaking waves, and $\hat{T}_m = 2$, which provides for a smooth acceleration of the body. The generated wave patterns in Fig. 7 seem realistic. In these computations, the total number of nodes was 4,879, with 1,844 nodes on the free surface and 306 nodes on the body surface. [Computations were performed on a Dell Optiplex GX240, which has an Intel Pentium 4, 1.5GHz processor, and 1 Gb of RAM. The total computation time was about 100 hours, with a memory requirement of about 430 Mb.]

To refine our computations and obtain accurate wave resistance coefficients, we will need to further refine the free surface grid. We will also perform computations for higher Froude numbers, for which generated waves will tend to break. In such cases, breaking will be prevented using the dissipation mechanism of Eqs. (19) and (20). These results of ongoing computations will be presented at the conference.

CONCLUSIONS

Numerical results obtained for both the traveling pressure patch and the Wigley hull show that the new TCD method is as accurate as the former Lagrangian method, while effectively reducing both domain size and computational cost. In computations, free surface nodes concentrate in some areas, due to Lagrangian flows; these are regridded onto a more regular grid at periodic intervals, to improve numerical accuracy.

ACKNOWLEDGEMENTS

The authors acknowledge support from a grant from Ocean Dynamics Inc (ODI), Wickford, RI, USA, awarded to the University of Rhode Island. The late John Hopkinson, President of ODI is recognized for his valuable insight with regard to this project. The first author's work was partially supported by the Post-doctoral Fellowship Program of the Korea Science and Engineering Foundation (KOSEF).

REFERENCES

Beck, R.F. (1999). "Fully nonlinear water wave computations using a desingularized Euler-Lagrange time domain approach," *In Nonlinear Water Wave Interaction* (O. Mahrenholtz and M. Markiewicz, Eds.), Advances in Fluid Mechanics Series, WIT Press, 1-58.

Beck, R. F. and A. M. Reed (2001). "Modern computational methods for ships in a seaway," *SNAME Transactions*, Vol 109, pp. 1-51.

Brandini, C. and S.T., Grilli (2001). "Modelling of freak wave generation in a three-dimensional NWT," *Proc. 11th Intl Offshore and Polar Engng Conf.*, Stavanger, Norway, Vol 3, pp 124-131.

Dawson , C. W. (1977). "A practical computer method for solving ship-wave problems," *Proc. 2nd Intl. Conf. Num. Ship Hydro.*, Berkeley, CA, pp 30-38.

Doctors, L. J. and S. D. Sharma (1972). "The Wave Resistance of an Air-Cushion Vehicle in Steady and Accelerated Motion," *J. Ship Res.*, Vol 16, pp 248-260.

Fochesato C. and Dias F. (2004) "Numerical model using the Fast Multipole Algorithm for nonlinear three-dimensional free-surface waves," (preprint CMLA).

Fochesato, C., Grilli, S. and Guyenne P. (2005) "Note on non-orthogonality of local curvilinear co-ordinates in a three-dimensional boundary element method," *Intl. J. Numer. Meth. In Fluids* (in press).

Grilli, S.T., P. Guyenne, and F. Dias (2000). "Modeling of overturning waves over arbitrary bottom in a 3D numerical wave tank," *Proc. 10th Intl Offshore and Polar Engng Conf.*, Seattle, USA, Vol 3, pp 221-228.

Grilli, S.T., Guyenne, P. and F., Dias (2001). "A fully nonlinear model for three-dimensional overturning waves over arbitrary bottom," *Intl J. Numer. Meth. Fluids*, Vol 35, pp. 829-867.

Grilli, S.T. and J. Horrillo (1997). "Numerical generation and absorption of fully nonlinear periodic waves," *J. Engng. Mech.*, Vol 123(10), pp 1060-1069.

Grilli, S.T. and R., Subramanya (1996). "Numerical modeling of wave breaking induced by fixed or moving boundaries," *Computational Mech.*, Vol 17, pp 374-391.

Hess J.L. and A. M.O. Smith (1964). "Calculation of nonlinear potential flow about arbitrary three-dimensional bodies," *J. Ship Res.*, Vol 8(2), pp 22-44.

Hinatsu, M. and T. Hino (2002). "Computation of viscous flow around a Wigley hull running in incident waves by use of unstructured grid method," *Proc. 12th Intl Offshore and Polar Engng Conf.*, Kitakyushu, Japan, Vol 3, pp 256-262.

Hino T. (1989). "Computations of a free surface flow around an advancing ship by the Navier-Stokes equations," *Proc. 5th Int. Conf. Num. Ship Hydro.* , pp 103-117.

Huang, Y. and P. D. Sclavounos (1998). "Nonlinear ship motions," *J. Ship Res.*, Vol 42(2), pp 120-130.

Jensen, G., V. Bertram and H. Söding (1989) "Ship wave-resistance computations," *Proc. 5th Intl. Conf. on Numer. Ship Hydr.*, Hiroshima, Japan , pp 593-606.

Liu Y., M. Xue and D. K. P. Yue (2001). "Computations of fully nonlinear tree-dimensional wave-wave and wave-body interactions. Part 2.," *J. Fluid Mech.*, Vol 438, pp. 41-66.

Longuet-Higgins, M.S. and E.D., Cokelet (1976). "The deformation of steep surface waves on water. I. A numerical method of computation," *Proc. R. Soc. Lond.* A, Vol 350, pp. 1-26.

Muscari, R. and A. Di Mascio (2004). "Numerical modeling of breaking waves generated by a ship's hull," *J. Marine Sc. and Tech.*, Vol 9, pp. 158-170.

Noblesse, F. (2000). "Analytical representation of ship waves," *23rd Weinblum Memorial Lecture*, Hydrodynamic Directorate Technical report NSWCCD-TR-2000/011, Naval Surface Warfare Center, Carderock Division.

Park J. C., Y. Uno, H. Matsuo, T. Sato and H. Miyata (2001). "Reproduction of fully-nonlinear multi-directional waves by a 3D viscous numerical wave tank," *Proc. 11th Intl Offshore and Polar Engng Conf.*, Stavanger, Norway, Vol 3, 140-147.

Pawloski, J. S. (1991). "A theoretical and numerical model of ship motions in heavy seas," *SNAME Transactions*, Vol 99, pp 319-352.

Raven, H.C. (1998) "Inviscid calculations of ship wave making-Capabilities, limitations, and prospects," *Proc. 22nd Symp. on Ship Hydr.*, Washington, D.C., pp 738-754.

Saad, Y. and Schultz, M.H. (1986). "GMRES: A generalized minimal residual algorithm for solving nonsymmetric linear systems," *SIAM J. Scient. Statistic Comp.*, Vol 7, pp. 856-869.

Sclavounos, P. D., D. C. Kring, Y. Huang, D. A. Mantzaris, S. Kim, and Y. Kim (1997). "A computational method as an advanced tool of ship hydrodynamic design," *SNAME Transactions*, Vol 105, pp 375-397.

Shirakura Y., K. Tanizawa and S. Naito (2000). "Development of 3-D fully nonlinear numerical wave tank to simulate floating bodies interacting with water waves," *Proc. 10th Intl Offshore and Polar Engng Conf.*, Seattle, USA, Vol 3, pp 253-262.

Tanizawa, K. (1996). "Nonlinear simulation of floating body motions in waves," *Proc. 6th Intl Offshore and Polar Engng Conf.*, Los Angeles, USA, Vol 3, 414-420.

Wehausen, J. V. (1973). "The wave resistance of ships," *Advances in Applied Mechanics*, Vol 13, pp 93-245.

Wyatt, D.C. (2000). "Development and assessment of a nonlinear wave prediction methodology for surface vessels," *J. Ship Res.*, Vol 44(2), pp 96-107.